Liquid-Crystalline Processing of Highly Oriented Carbon Nanotube Arrays for Thin-Film Transistors

Hyunhyub Ko[†] and Vladimir V. Tsukruk*,[†,‡]

Materials Science & Engineering Department, Iowa State University, Ames, Iowa 50011, and School of Materials Science and Engineering, Georgia Institute of Technology, Atlanta, Georgia 30332

ABSTRACT

We introduce a simple solution-based method for the fabrication of highly oriented carbon nanotube (CNT) arrays to be used for thin-film transistors. We exploit the liquid-crystalline behavior of a CNT solution near the receding contact line during tilted-drop casting and produced long-range nematic-like ordering of carbon nanotube stripes caused by confined micropatterned geometry. We further demonstrate that the performance of thin-film transistors based on these densely packed and uniformly oriented CNT arrays is largely improved compared to random CNTs. This approach has great potential in low-cost, large-scale processing of high-performance electronic devices based on high-density oriented CNT films with record electrical characteristics such as high conductance, low resistivity, and high career mobility.

Electronic devices based on solution-processable one-dimensional semiconducting materials and their arrays are generating significant research interest for the applications requiring low-cost fabrication, large-area coverage, and low-temperature processing on flexible substrates.[1−3] Semiconducting single-wall carbon nanotubes (SWNTs) are one of the promising candidates for high-performance thin-film transistors (TFTs) because of their potentially high carrier mobilities and large current-carrying capacities.[4,5] However, because of the limited current-carrying capacity of individual SWNTs, random networks or parallel arrays of SWNTs would be required to provide the necessary current density of devices. The performance of carbon nanotube (CNT) TFTs can be improved by increasing the surface density and controlling the uniform alignment of CNTs. Several approaches have been made to align CNTs by solution-based techniques,[6−12] but most of the methods are limited in their prospective applications because of the low surface density of the CNT array formed. Other solution-based approaches have been attempted to make highly dense CNTs, but the resulting CNT layer is randomly oriented.[13]

Highly dense, randomly oriented CNTs have been used recently as effective semiconducting layers for thin-film transistors, although the inter-nanotube contact resistance of many overlapping tubes limited the full exploitation of the intrinsic high mobilities.[14−18] Recently, it has been demon-strated that carbon nanotubes, like other anisotropic and one-dimensional molecules, might form a lyotropic liquid-crystalline phase.[19−22] Above a critical concentration, CNTs have shown a phase transition to the nematic liquid-crystal phase. This liquid-crystalline behavior of CNT solution can offer novel solution-processable routes to large-scale alignment of CNTs in many potential applications requiring oriented CNT arrays.[23] However, inducing long-range nematic ordering with low misaligned defects within the CNT surface layer still remains a big challenge.

Herein, we report the formation of long-range ordered and dense arrays of CNTs via liquid-crystalline processing by simple tilted-drop casting of CNT solution on functionalized micropatterned geometries. As the solvent evaporates during tilted-drop casting, the carbon nanotubes diffuse from the bulk solution to the liquid−solid−air receding contact line by convective flow, causing the concentrated solution to form a nematic liquid-crystalline phase. The confined geometry of the micropatterned surface induces a uniform long-range orientation of dense CNT films during the surface deposition. We further demonstrate that the electrical performance of thin-film transistors based on these densely packed uniformly oriented CNT array is improved dramatically compared to random CNTs.

Purification of single-wall carbon nanotubes synthesized by arc-discharge (Carbon Solutions, Inc) was performed by mild air oxidation (350 °C, 2 h), followed by a 6 M hydrochloric acid washing for 2 h. Stable dispersion of CNTs was achieved by dissolving purified CNTs in 1% aqueous

---

* To whom correspondence should be addressed. E-mail: vladimir@iastate.edu.
† Iowa State University.
‡ Georgia Institute of Technology.
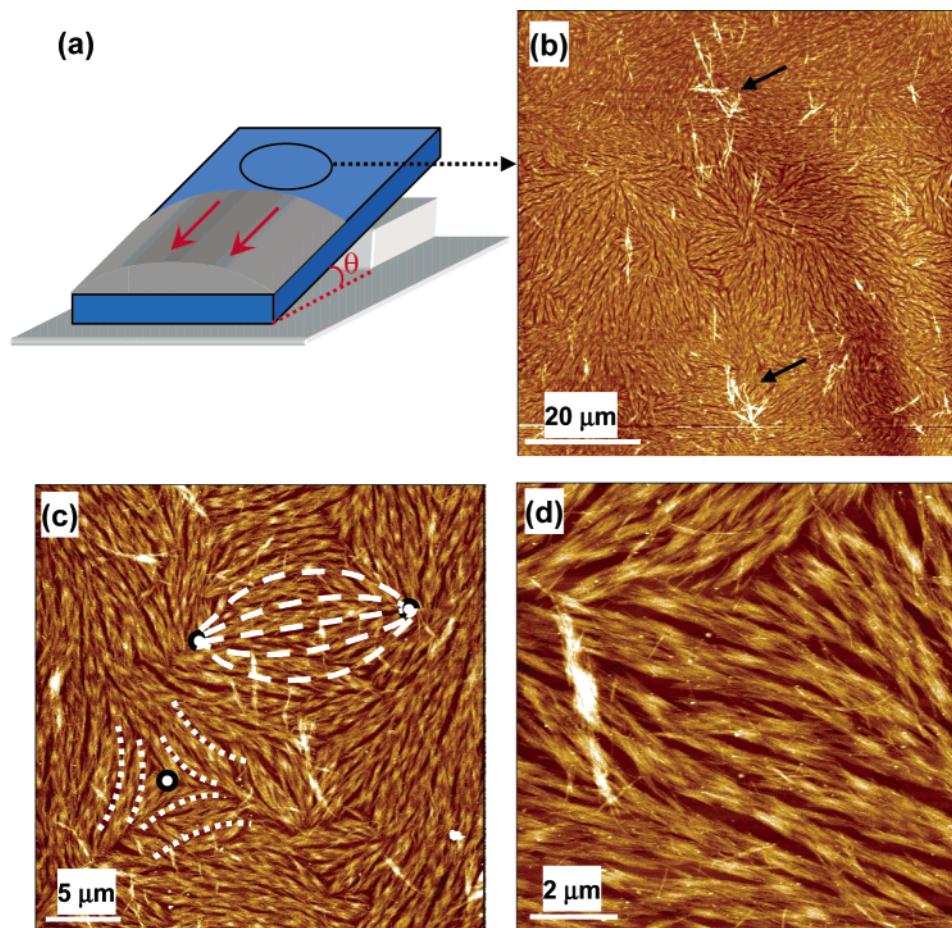
Figure 1. Surface ordering of carbon nanotube films by slow evaporation of carbon nanotube solution during tilted-drop casting on the NH₂-terminated SAM surface of a silicon wafer. (a) Scheme for the tilted-drop fabrication routine without physical confinement. (b–d) AFM topographical images of a CNT surface film at different magnifications showing liquid-crystalline texture and ordering along with characteristic topological defects.

sodium dodecyl sulafate (SDS) solution by sonication for 2 h and centrifugation (18 000 rpm, 1 h). The resulting SWNT bundles were 1.6 ± 0.6 μm in length and 6.7 ± 3.0 nm in diameter, as measured from atomic force microscopy (AFM).[24] The concentration of the resulting CNT solution was ∼0.1–0.2 mg/mL. All of the silicon substrate was modified with (aminopropyl)triethoxysilane to form an NH₂-terminated surface. The CNT solution was tilted-drop cast on photo-lithographically patterned surfaces tilted about 5° for uni-directional solvent evaporation. The tilted-drop casting process was conducted in a sealed container (within 2 days) for SWNT films in Figure 1 or in ambient laboratory conditions (within 18 h) without using any sealed container for other SWNT films. For CNT-TFT fabrication, a heavily doped silicon wafer was used as the substrate and the gate electrode. CNT films were fabricated on a SiO₂ (200 nm)/ Si substrate, and, subsequently, Au electrodes were prepared with e-beam lithography followed by lift-off of photoresist (AZ 5214). The semiconducting properties of CNT-TFTs were measured by a HP 4155 semiconductor parameter analyzer for 5–7 devices with variable channel lengths and presented as average values.

Figure 1a shows a schematic of the tilted-drop casting process of SWNT solution on a silicon wafer modified with a NH₂-terminated self-assembled monolayer (SAM) accord-ing to the procedure described in detail elsewhere.[24,25] For this process, an appropriate amount of SWNT solution was spread on the tilted substrate and left without any perturbation inside a sealed container. As the solvent evaporated, the liquid−solid−air contact line swept down the surface, accumulating highly concentrated solution in the vicinity and leaving a dense CNT layer behind the receding line. Figure 1b shows an AFM image of the resulting SWNT film formed after tilted-drop casting was completed. It shows a large area of dense SWNT film in which SWNT bundles form a monolayer surface film with the thickness 7 nm close to the diameter of the bundles (Supporting Information Figure S1) with occasional defects and multilayer aggregates (indicated by arrows).

A higher resolution imaging revealed that SWNTs are assembled into small bundle-like structures and within each domain SWNTs are uniformly aligned (Figure 1c and d). This microstructure is similar to nematic-type ordering observed for liquid-crystalline CNT solutions and their footprints on a solid substrate.[21,26,27] Although previous studies are based on highly concentrated CNT solutions, our observed liquid-crystalline-like surface structures are achieved from low-concentration (∼0.1−0.2 mg/mL) aqueous solution
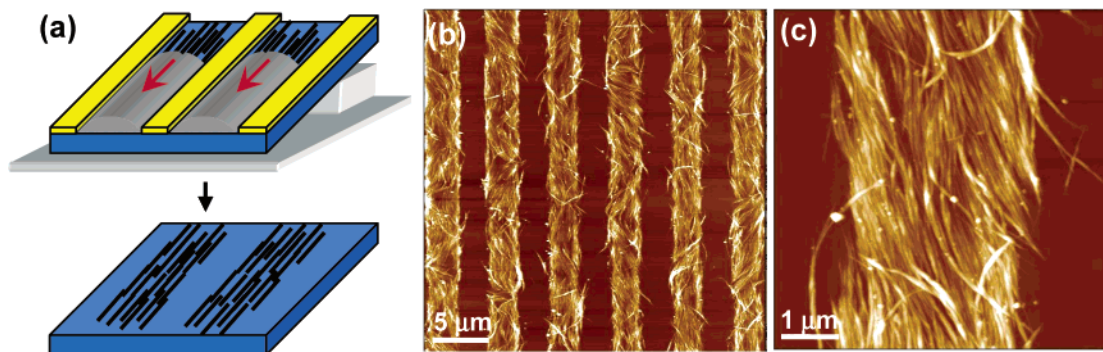
Figure 2. (a) Schemes for the tilted-drop fabrication of a thin film on an amine-terminated SAM surface micropatterned with photoresist polymer stripes. (b and c) AFM topographical images of carbon nanotube films showing uniaxially oriented, densely packed CNT bundles.

but involves ordering along the receding contact line. We suggest that the formation of the liquid-crystalline structure is caused by the high evaporation rate on the contact line, resulting in highly concentrated solution in the vicinity of the receding contact line, thus promoting the liquid-crystalline ordering. This phenomenon is well known in colloid systems,[28,29] and a similar behavior has been observed previously for SWNT[30,31] and nanorod solutions.[32,33]

The surface textures and defects for our SWNTs closely resemble those observed for liquid-crystalline CNTs.[20,31] The typical singularity defects of liquid-crystalline types related to disclinations with a singular center and with two centers are presented in Figure 2c. It is worth noting that by changing the solvent evaporation rate the structure of the SWNT film can be controlled: with increasing the evaporation rate, the size of nematic-type domain decreased, resulting in an isotropic texture when the evaporation completed within several hours (Supporting Information Figure S2). Consequently, the higher nematic ordering is achieved by slowing down the solvent evaporation rate. Finally, surface cracks and undulations observed for these CNT films occur because of internal stresses from the coupling between the nematic ordering and elasticity in the formation process.[20]

The array of long-range nematic structures can be created by confining the drying process within micropatterned geometries (Figure 2a). To control this process, we formed stripes of photoresist on top of amine-terminated SAM by using photolithography with the periodicity 5 μm. In this case, the tilted-drop casting process splits in parallel microchannels with the solution confined between parallel solid walls (height is 1.3 μm) (Figure 2a). This modification results in a unidirectional microfluidic flow pattern, which causes the formation of multiple stripes of highly oriented SWNT films. Removing the photoresist micropattern leads to the densely packed oriented SWNT stripes with 2.5 μm width and 5 μm periodicity (Figure 2b and c). Within these stripes, SWNTs form undulated structures with the director of the local orientation regularly modulating along the axis due to capillary instabilities in the receding front.[34] It is worth noting that when the width of confining channel increased and became much higher than the average nanotube length (1.6 μm) the nematic-like ordering vanished. This behavior indicates the importance of the steric factors in the formation of highly oriented structures.

These dense and highly oriented SWNT films can be exploited as components in high-performance electronic devices. Without going into detailed study of the device performance, but just to test their potential, we fabricated CNT thin-film transistors (TFTs) in which densely packed CNT layers serve as semiconducting channels between source and drain electrodes (Figure 3a and b). For device fabrication, source−drain contact electrodes were made with Au (50 nm high) layers by using e-beam evaporation and a subsequent lift-off process. Here, we used only an Au contact with a minimal Schottky barrier to carbon nanotubes.[35] As known, Au electrodes are strongly attached to the silicon surface because of the affinity to amine-terminated SAM and the use of an additional interlayer can be avoided, making the fabrication process simpler without compromising structure robustness.

To analyze the preliminary electrical properties and device performances, we fabricated oriented and random CNT films that were formed with and without micropatterning, respectively (Figure 3c and d). CNT surface layers with confined geometries show strong preferential orientation with some modulation along the stripes due to flow instabilities while random texture was observed in traditional CNT film (Figure 3c and d). The nanotube density in both cases was about 18 bundles/μm, which corresponds to a surface density of 7 bundles/μm^2, taking into account of the average bundle length (1.6 μm).

The transfer and output characteristics of a CNT-TFT are shown in Figure 4a and b. The device exhibits p-type semiconducting behavior with a linear IV_{ds} characteristics and minor IV_g hysteresis, which is a typical behavior of SWNT transistors operated in air.[37] The saturation regime was not reached under experimental conditions available. Also, the device shows a modest dependence on gate voltage due to the presence of CNT bundles containing metallic nanotubes. The transistor with random SWNTs shows similar p-type semiconducting behavior, but the current level is much lower than that of oriented SWNTs (see the inset in Figure 4a). The electrical characteristics are compared in Figure 4c−f for CNT-TFTs with different channel lengths (different distances between electrodes). Considering that the effective channel width contributing to the observed transport properties is half of the full channel width (200 μm) for a micropatterned array, we normalized the device performances
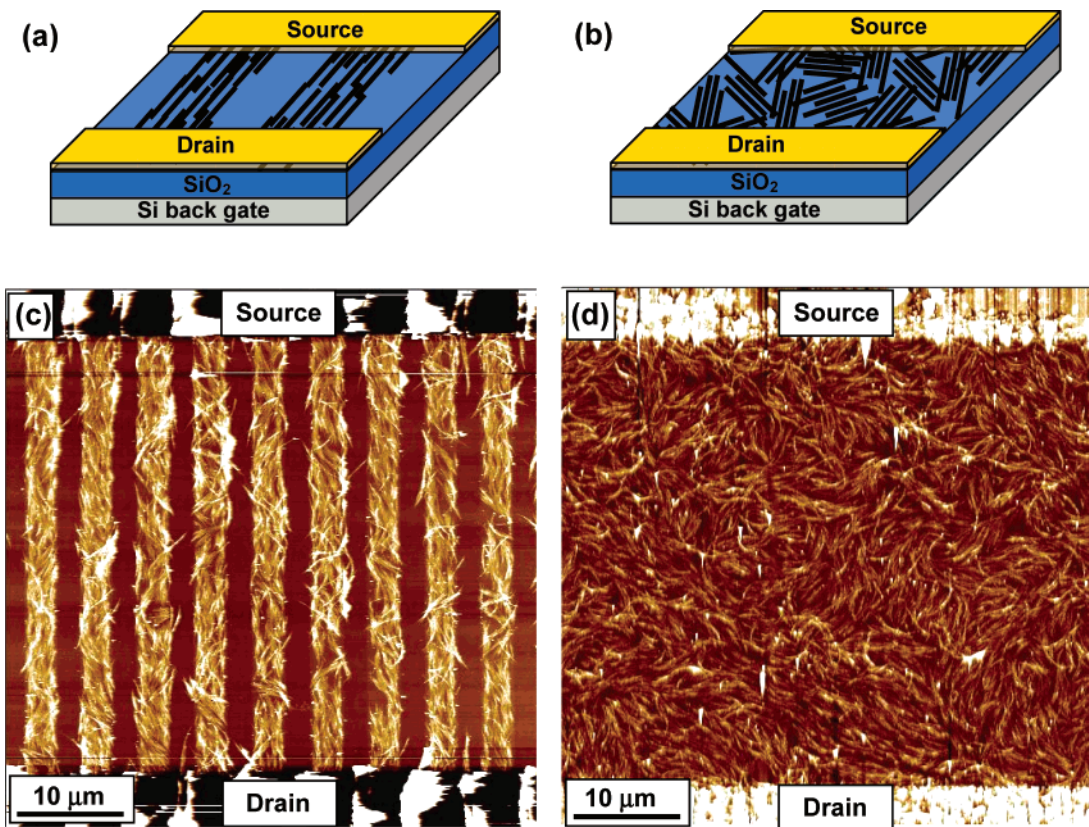
Figure 3. Device configurations of back-gated oriented (a) and random CNT-TFTs (b) with Au source/drain electrodes. (c) AFM topographical image of a CNT-TFT with uniaxially ordered micropatterned CNT array. (d) AFM topographical image of a CNT-TFT with randomly oriented CNT surface film.

(conductance, mobility, and transconductance) correspondingly. As can be seen in Figure 4c, the resistance of the oriented CNT-TFT is much lower (3−5 times) than that with a random CNT surface layer. Moreover, the contact resistances of the gold/nanotube interface, as determined by the y intercept of the linear fit, are negligible compared to the channel resistances, indicating an excellent property achieved by avoiding the use of adhesive metal interlayers.

Correspondingly, the normalized conductance of oriented CNT-TFTs is 4−7 times higher than those with random CNTs (Figure 4d). All CNT-TFTs show a similar linear dependence of conductance upon channel length with the conductance exponent of −1.17 for oriented and −0.96 for random CNT-TFTs. The value of −0.96 for random SWNT film agrees very well with the experimental and theoretical studies based on random network of SWNT films.[14,36] As known, the conductance exponent approaches −1.0 for high-density (>3.0 μm^2) SWNT films and decreases with decreasing nanotube density.[36] Oriented CNT-TFTs possess similar conductance exponents with some higher-off deviation on channel 2.5 μm, which is possibly caused by the occasional ballistic transport through highly oriented longer nanotubes (over 2-3 μm) for short channel length (2.5 μm). As known, the ballistic transport for short channel length can make the transport scaling more rapidly with channel length.[14,36]

The linear hole mobility estimated from the relation $\mu = (dI_D/dV_G)(L/WCV_D)$, where I_D is the drain current, V_G is the gate voltage, L is the channel length, W is the channel width,

C is the gate capacitance, and V_D is the drain voltage, is presented in Figure 4e.[18] The gate capacitance can be estimated from the relation $C = \epsilon\epsilon_0/t$, where ϵ is the dielectric constant of the silicon oxide (3.9), ϵ_0 is the vacuum permittivity, and t is the thickness of the gate dielectric (silicon oxide).[18] The hole mobility increases with the channel length in the short channel range until saturation for the long channels. The hole mobility of oriented CNT-TFT is in the range of 60−92 cm^2/Vs, which is much larger (5−6 times) than those of random CNT-TFTs. Both values are significantly larger than those of amorphous Si TFTs (<1 cm^2/Vs).[37] We suggest that the uniaxially oriented SWNTs significantly reduce the number of inter-tube contacts that the carriers should pass through, resulting in dramatically increased mobility. The highest mobility of 126 cm^2/Vs achieved for some oriented CNT-TFTs (for channel length of 20 μm, see the data in Supporting Information Figure S3) is comparable to the record mobility reported for the highly oriented SWNT TFTs (125 cm^2/Vs) prepared by the CVD method.[38] However, this mobility is higher than those for the TFTs with parallel arrays of silicon nanowires (119 cm^2/Vs).[39]

Finally, normalized device transconductance ($g_m=(dI_D/dV_G)/W$) scales linearly with channel length for both TFTs (Figure 4f). The transconductance is within 0.02 − 0.2 $\mu S/\mu m$ (at $V_D = 0.1$ V) for oriented CNT-TFTs, which is 7 times higher than that for random CNT-TFTs (0.003−0.03 $\mu S/\mu m$). The transconductance value (0.02−0.2 $\mu S/\mu m$) for
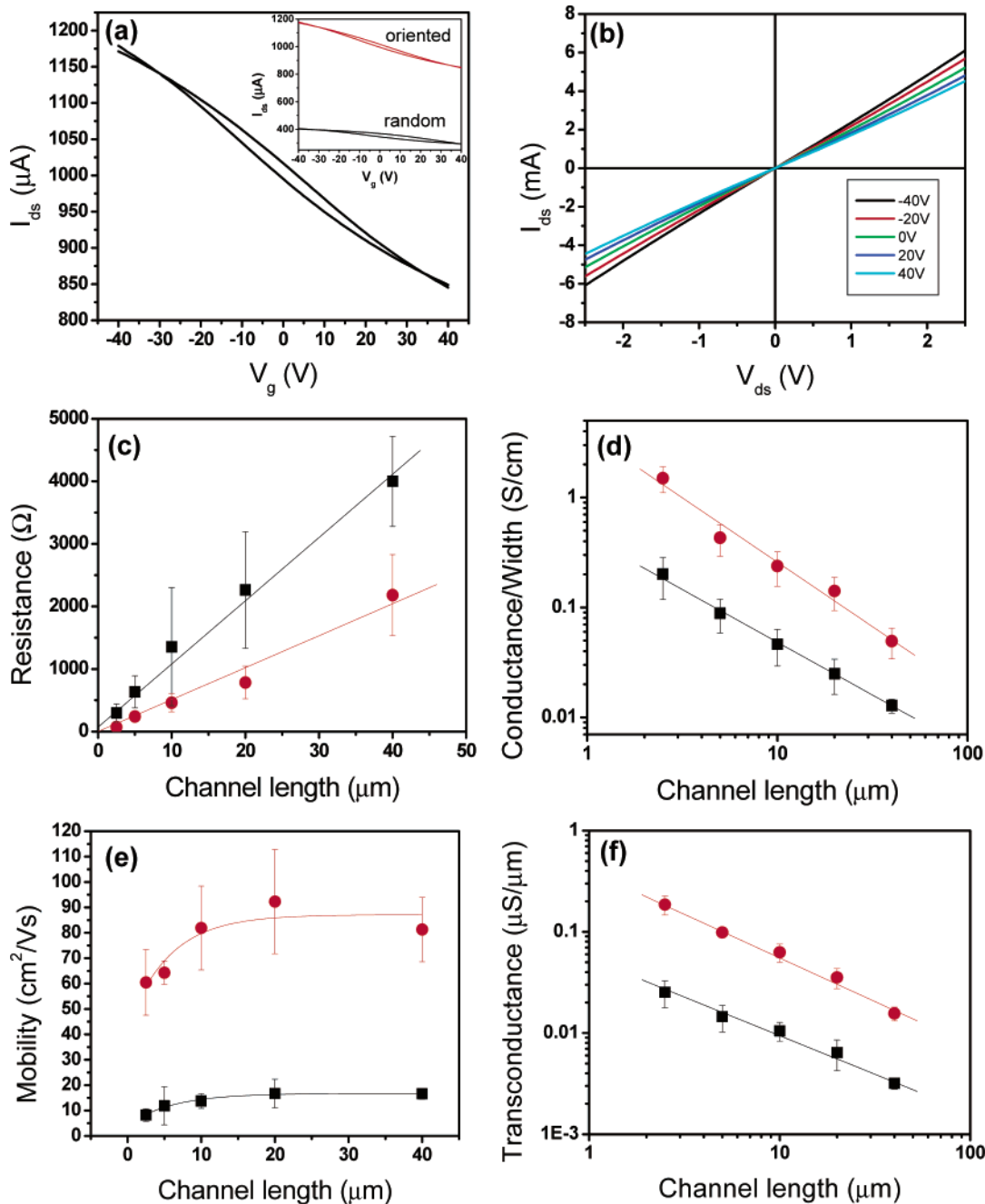
Figure 4. (a) Transfer characteristics of oriented CNT-TFTs with 20 mm channel length. The bias voltage, V_{ds}, is 0.5 V. The inset compares the transfer characteristics between oriented and random SWNTs. (b) Output characteristics of oriented CNT-TFTs when the gate voltage is swept from −40 to 40 V in 20 V steps. (c−f) Electrical characteristics of oriented (circles) and random (squares) CNT-TFTs with different channel lengths: (c) resistance measured at V_{gs} = −40 V; (d) normalized conductance measured at V_{gs} = −40 V, channel width is 200 μm; (e) career mobility; (f) normalized transconductance.

oriented CNT-TFTs is higher/comparable to that of oriented Si nanowire TFTs (0.09 μS/μm).[39] These and other electrical characteristics of oriented CNT-TFTs quoted above are much higher than those for random CNT-TFTs. Moreover, they are very high compared to the usual literature values for CNT-TFTs and are sometimes close to the record values reported for rather complicated TFT versions.

In conclusion, we have developed a simple and easy solution-based assembly strategy for the fabrication of densely packed, uniaxially aligned SWNTs as a semiconducting layer in CNT-TFTs. We suggested using the liquid-

crystalline behavior of CNT solution in the vicinity of the receding contact line induced by localized solvent vaporization. We have controlled the nematic-like ordering of carbon nanotubes during the tilted-drop casting process by using a confined micropatterned geometry. Because of the liquid-crystalline behavior near the contact line, the process suggested does not require highly concentrated CNT solution and still provides for densely packed and uniformly oriented CNT predominantly monolayer surface films.

Although our CNT-TFTs show excellent electrical characteristics even without special optimization, their relatively

low on/off ratios (<3) are caused by the presence of metallic SWNTs in the semiconducting channels because of the mixed character of CNTs used here. However, the high device mobility and transconductance values demonstrate the potential application of high-density oriented SWNT films in low-cost, large-scale, high-performance electronic devices.[1,40] Prospective realization of high-performance CNT-TFTs will rely on the electronic purity of SWNTs, which should be addressed in future studies. These issues are currently tackled by several research groups working toward the effective separation of metallic and semiconducting nanotubes.[41,42] We believe that if highly purified carbon nanotubes will be exploited then the tilted-drop approach suggested here will be instrumental in a simple fabrication of highly efficient thin-film transistors and other electronic microdevices with breakthrough electronic characteristics.

Supporting Information Available: Data on carbon nanotube ordering under different conditions and additional conductivity data. This material is available free of charge via the Internet at http://pubs.acs.org.

References

(1) Forrest, S. R. *Nature* **2004**, *428*, 911.
(2) Mitzi, D. B. *J. Mater. Chem.* **2004**, *14*, 2355.
(3) Whang, D.; Jin, S.; Wu, Y.; Lieber, C. M. *Nano Lett.*, **2003**, *3*, 1255.
(4) Durkop, T.; Getty, S. A.; Cobas, E.; Fuhrer, M. S. *Nano Lett.* **2004**, *4*, 35.
(5) Yao, Z.; Kane, C. L.; Dekker, C. *Phys. Rev. Lett.* **2000**, *84*, 2941.
(6) Gao, J. B.; Yu, A. P.; Itkis, M. E.; Bekyarova, E.; Zhao, B.; Niyogi, S.; Haddon, R. C. *J. Am. Chem. Soc.* **2004**, *126*, 16698.
(7) McLean, R. S.; Huang, X. Y.; Khripin, C.; Jagota, A.; Zheng, M. *Nano Lett.* **2006**, *6*, 55.
(8) Wang, Y.; Maspoch, D.; Zou, S.; Schatz, G. C.; Smalley, R. E.; Mirkin, C. A. *Proc. Natl. Acad. Sci. U.S.A.* **2006**, *103*, 2026.
(9) Lay, M. D.; Novak, J. P.; Snow, E. S. *Nano Lett.* **2004**, *4*, 603.
(10) Meitl, M. A.; Zhou, Y. X.; Gaur, A.; Jeon, S.; Usrey, M. L.; Strano, M. S.; Rogers, J. A. *Nano Lett.* **2004**, *4*, 1643.
(11) Shim, B. S.; Kotov, N. A. *Langmuir* **2005**, *21*, 9381.
(12) Xin, H. J.; Woolley, A. T. *Nano Lett.* **2004**, *4*, 1481.
(13) Park, J. U.; Meitl, M. A.; Hur, S. H.; Usrey, M. L.; Strano, M. S.; Kenis, P. J. A.; Rogers, J. A. *Angew. Chem., Int. Ed.* **2006**, *45*, 581.
(14) Snow, E. S.; Novak, J. P.; Campbell, P. M.; Park, D. *Appl. Phys. Lett.* **2003**, *82*, 2145.
(15) Bradley, K.; Gabriel, J. C. P.; Gruner, G. *Nano Lett.* **2003**, *3*, 1353.
(16) Seidel, R.; Graham, A. P.; Unger, E.; Duesberg, G. S.; Liebau, M.; Steinhoegl, W.; Kreupl, F.; Hoenlein, W. *Nano Lett.* **2004**, *4*, 831.
(17) Zhou, Y. X.; Gaur, A.; Hur, S. H.; Kocabas, C.; Meitl, M. A.; Shim, M.; Rogers, J. A. *Nano Lett.* **2004**, *4*, 2031.
(18) Ozel, T.; Gaur, A.; Rogers, J. A.; Shim, M. *Nano Lett.* **2005**, *5*, 905.
(19) Badaire, S.; Zakri, C.; Maugey, M.; Derre, A.; Barisci, J. N.; Wallace, G.; Poulin, P. *Adv. Mater.* **2005**, *17*, 1673.
(20) Islam, M. F.; Nobili, M.; Ye, F. F.; Lubensky, T. C.; Yodh, A. G. *Phys. Rev. Lett.* **2005**, *95*, 148301.
(21) Song, W. H.; Kinloch, I. A.; Windle, A. H. *Science* **2003**, *302*, 1363.
(22) Davis, V. A.; Ericson, L. M.; Parra-Vasquez, A. N. G.; Fan, H.; Wang, Y. H.; Prieto, V.; Longoria, J. A.; Ramesh, S.; Saini, R. K.; Kittrell, C.; Billups, W. E.; Adams, W. W.; Hauge, R. H.; Smalley, R. E.; Pasquali, M. *Macromolecules* **2004**, *37*, 154.
(23) Ericson, L. M.; Fan, H.; Peng, H. Q.; Davis, V. A.; Zhou, W.; Sulpizio, J.; Wang, Y. H.; Booker, R.; Vavro, J.; Guthy, C.; Parra-Vasquez, A. N. G.; Kim, M. J.; Ramesh, S.; Saini, R. K.; Kittrell, C.; Lavin, G.; Schmidt, H.; Adams, W. W.; Billups, W. E.; Pasquali, M.; Hwang, W. F.; Hauge, R. H.; Fischer, J. E.; Smalley, R. E. *Science* **2004**, *305*, 1447.
(24) Ko, H.; Peleshanko, S.; Tsukruk, V. V. *J. Phys. Chem. B* **2004**, *108*, 4385.
(25) Tsukruk, V. V.; Ko, H.; Peleshanko, S. *Phys. Rev. Lett.* **2004**, *92*, 065502.
(26) Zhang, S.; Kinloch, I. A.; Windle, A. H. *Nano Lett.* **2006**, *6*, 568.
(27) Ramesh, S.; Ericson, L. M.; Davis, V. A.; Saini, R. K.; Kittrell, C.; Pasquali, M.; Billups, W. E.; Adams, W. W.; Hauge, R. H.; Smalley, R. E. *J. Phys. Chem. B* **2004**, *108*, 8794.
(28) Deegan, R. D.; Bakajin, O.; Dupont, T. F.; Huber, G.; Nagel, S. R.; Witten, T. A. *Nature* **1997**, *389*, 827.
(29) Kim, M. H.; Im, S. H.; Park, O. O. *Adv. Funct. Mater.* **2005**, *15*, 1329.
(30) Shimoda, H.; Oh, S. J.; Geng, H. Z.; Walker, R. J.; Zhang, X. B.; McNeil, L. E.; Zhou, O. *Adv. Mater.* **2002**, *14*, 899.
(31) Duggal, R.; Hussain, F.; Pasquali, M. *Adv. Mater.* **2006**, *18*, 29.
(32) Nikoobakht, B.; Wang, Z. L.; El-Sayed, M. A. *J. Phys. Chem. B* **2000**, *104*, 8635.
(33) Li, L. S.; Alivisatos, A. P. *Adv. Mater.* **2003**, *15*, 408.
(34) Reiter, G.; Sharma, A. *Phys. Rev. Lett.* **2001**, *87*, *166103*.
(35) Yaish, Y.; Park, J. Y.; Rosenblatt, S.; Sazonova, V.; Brink, M.; McEuen, P. L. *Phys. Rev. Lett.* **2004**, *92*, 046401.
(36) Kumar, S.; Murthy, J. Y.; Alam, M. A. *Phys. Rev. Lett.* **2005**, *95*, 066802.
(37) Kagan, C. R.; Andry, P. *Thin-Film Transistors*; Marcel Dekker: New York, 2003.
(38) Kocabas, C.; Hur, S. H.; Gaur, A.; Meitl, M. A.; Shim, M.; Rogers, J. A. *Small* **2005**, *1*, 1110.
(39) Duan, X. F.; Niu, C. M.; Sahi, V.; Chen, J.; Parce, J. W.; Empedocles, S.; Goldman, J. L. *Nature* **2003**, *425*, 274.
(40) Dimitrakopoulos, C. D.; Malenfant, P. R. L. *Adv. Mater.* **2002**, *14*, 99.
(41) Strano, M. S.; Dyke, C. A.; Usrey, M. L.; Barone, P. W.; Allen, M. J.; Shan, H. W.; Kittrell, C.; Hauge, R. H.; Tour, J. M.; Smalley, R. E. *Science* **2003**, *301*, 1519.
(42) Zheng, M.; Jagota, A.; Strano, M. S.; Santos, A. P.; Barone, P.; Chou, S. G.; Diner, B. A.; Dresselhaus, M. S.; McLean, R. S.; Onoa, G. B.; Samsonidze, G. G.; Semke, E. D.; Usrey, M.; Walls, D. J. *Science* **2003**, *302*, 1545.

NL060608R